

SAND78-8256  
Unlimited Release

## Corrosion of Fe Alloys in HITEC at 823 K

C. M. Kramer, W. H. Smyrl, and W. B. Estill

Prepared by Sandia Laboratories, Albuquerque, New Mexico 87115  
and Livermore, California 94550 for the United States Department  
of Energy under Contract AT(29-1)-789.

Printed February 1979



Sandia Laboratories

SF 2900 Q(7-73)

***When printing a copy of any digitized SAND Report, you are required to update the markings to current standards.***

Issued by Sandia Laboratories, operated for the United States Department of Energy by Sandia Corporation.

---

---

#### NOTICE

This report was prepared as an account of work sponsored by the United States Government. Neither the United States nor the United States Department of Energy, nor any of their employees, nor any of their contractors, subcontractors, or their employees, makes any warranty, express or implied, or assumes any legal liability or responsibility for the accuracy, completeness or usefulness of any information, apparatus, product or process disclosed, or represents that its use would not infringe privately owned rights.

Printed in the United States of America  
Available from  
National Technical Information Service  
U. S. Department of Commerce  
5285 Port Royal Road  
Springfield, VA 22161  
Price: Printed Copy \$4.50 ; Microfiche \$3.00

SAND78-8256  
Unlimited Release  
Printed February 1979

CORROSION OF Fe ALLOYS  
IN HITEC AT 823K

C. M. Kramer  
Exploratory Chemistry Division I 8313

W. H. Smyrl  
Chemical Metallurgy Division 5831

W. B. Estill  
Materials Science Division 8316

ABSTRACT

In support of advanced solar central receiver programs, six commercially available, iron-based construction materials were exposed to molten  $\text{NaNO}_2$ - $\text{NaNO}_3$ - $\text{KNO}_3$  salt at 823K for periods up to 6 months. After 1 month of exposure, oxide coatings had formed on each alloy; the amount of oxidation ranged from  $10 \text{ mg/cm}^2$  for low carbon steel to  $\sim 0.1 \text{ mg/cm}^2$  for 310 stainless steel. Analysis of the oxide surface of a 5% chrome alloy indicated a chromia enriched layer was present at the oxide/metal interface. An iron oxide rich layer was present at the outer oxide surface which contacted the molten salt.

## CONTENTS

	<u>Page</u>
Introduction	7
Experimental Technique	10
Results and Discussion	10
Conclusions	13
References	30

## ILLUSTRATIONS

<u>Figure</u>		<u>Page</u>
1.	Schematic of Molten Salt Bath	14
2.	Oxidation of 1018 and Stainless Steels	15
3.	Oxidation of Low-Cr Fe Alloys	16
4.	Oxidation Versus Cr Content	17
5.	Macro Photo of Corroded Coupons	18
6.	Cross-sectional Views of Corroded Coupons	19
7.	Topographical Photos of Oxide Coatings	20
8.	Electron Microprobe Maps of Corrosion Interfaces	21
9.	Electron Microprobe Concentration Profiles	22
10.	Oxidation of Metals in Air and Hitec	23

## TABLES

I.	Chemical Composition of Alloys	24
II.	Sample Dimensions	25
III.	Oxidation of Fe-Alloys	26
IV.	Rate Constants for Oxidation of Iron Alloys	27
V.	Chemical Composition of Molten Salt Bath	28

## Introduction

Molten Hitec\*<sup>®</sup> has been proposed as the primary heat transfer fluid for a solar large power system<sup>1</sup>. The potential corrosion of metals by the molten Hitec salt was a major concern. The corrosion of iron, chrome, nickel, cobalt, and some iron alloys in molten nitrates and nitrites has been studied<sup>2-8</sup>. In general, metals in molten nitrates and nitrites are passivated by the formation of oxide films. It has been found that the oxide film thickness can be increased by mild anodic conditions, but iron for example shows transpassive corrosion behavior under strong anodic conditions<sup>4,9</sup>. Cathodic conditions cause the oxide film thickness to decrease, and lead to catastrophic destruction of the film on stainless steel and very severe corrosion<sup>10\*\*</sup>. These tests were conducted at lower temperatures than expected for the solar large power systems and only for short times (up to 6 weeks). The data were considered inadequate for making a materials recommendation for the solar system; therefore this program was started to evaluate the compatibility of molten Hitec with several metals under the condition of interest.

The corrosion behavior of a metal is determined by the relative thermodynamic stability of the metal and the environment, and also by the rate of the corrosion reactions if any occur. Plambeck<sup>11</sup> has reviewed the thermodynamic properties of metals in several molten salts, and has summarized the data in the form of electrode potential series in each molten salt (see also Boxall, et al.<sup>12</sup>. For molten chlorides and fluorides, the stability of metals is almost completely determined by thermodynamics because oxide films are not protective and provide no passivity in these melts. In molten nitrates on the other hand, the stability is almost completely kinetic because of the strong oxidizing ability of the nitrates.

The thermodynamic properties of several metals in molten nitrate melts have been summarized in the form of electrode potential (E) versus the concentration of oxide ions (as  $pO^{2-}$ ). The larger the concentration of oxide ions, the more basic is the melt in the Lux-Flood sense. However, there is controversy concerning the nature of the basic species in nitrate melts. Plambeck<sup>13</sup> has summarized the recent work in which peroxide as well as superoxide ions are present, and these are in concentrations large compared to

---

\*53 wt.%  $KNO_3$ , 40wt.%  $NaNO_2$ , 7 wt.%  $NaNO_3$ , MP = 415K.

<sup>®</sup>Registered trademarks of E. I. duPont de Nemours Co., Inc.

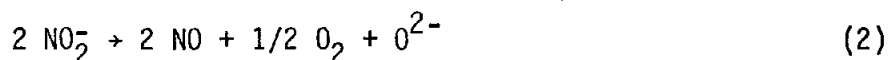
\*\*We have also found that Cr metal may be "activated" and caused to corrode severely under cathodic conditions.

the oxide concentration. This suggests that the redox properties of the melts will be strongly influenced by the peroxide and superoxide, but the acid-base reactions will involve the oxide ion. Some stability diagrams have been constructed however using  $pO_2^{2-}$  and  $pO_2^-$  instead of  $pO^{2-}$  14.

This introductory discussion will be concluded with a description of the chemistry of nitrates and nitrites, especially as related to the present investigation. The stability of the nitrates has been measured with respect to thermal decomposition. Both kinetic and equilibrium measurements have been made. The nitrates decompose at low temperatures<sup>15,16</sup> according to (1).



At 573K, the equilibrium concentration of nitrite was found to be  $2 \times 10^{-4}$  mole at 0.85 atm  $O_2$  in  $NaNO_3/KNO_3$ . Nitrites decompose according to



where the oxide has been used to designate the basic species in solution, although other species are expected as discussed above. Melts starting with nitrite would be expected to be quite basic due to self ionization as well, that is, the nitrite may generate oxide ion according to (3).

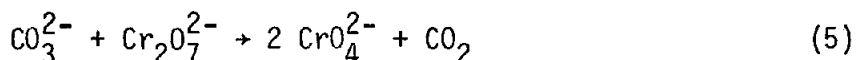


The equilibrium constant determined for this reaction was approximately  $10^{-9}$  at 573K, although it must be regarded as tentative. Melts which start with nitrite would be expected to change composition as the nitrite decomposes, and pure nitrates will produce some nitrite by thermal decomposition as well. This suggests that the final melt may be rather similar in each case. Melts with large concentrations of nitrite may attack materials which are sensitive to oxide ions.

There are other types of acid-base behavior which may be important with regard to corrosion including reaction with ambient carbon dioxide, as below.



The solubility of carbonate has been measured in  $NaNO_3/KNO_3$  17, and several other nitrates and nitrites as well<sup>18</sup>. The addition of dichromate to a melt containing carbonate would yield chromate as in equation (5).

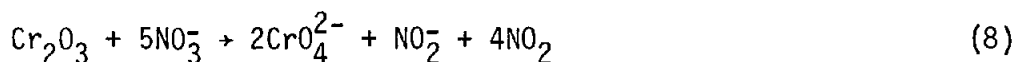
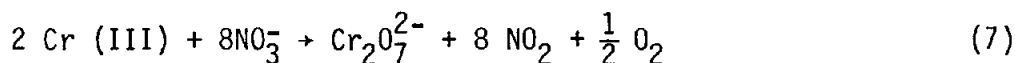


This suggests a means of controlling the concentration of carbonate.\* The reaction of some metal oxides with excess oxide can cause the formation of soluble species according to (6) or a similar reaction.



This would limit the passivity and protection of such oxides, although it is unlikely to be of importance for any of the materials of this study.

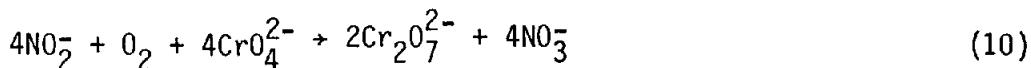
The redox chemistry of the melt reflects the strong oxidizing properties of the melt, so that Cr (III) is not stable in the melt but is oxidized according to reaction (7) or (8)<sup>13</sup>.



Also, nitrate solutions of chromate and dichromate are quite stable and act as oxide buffers because of reaction (9).



The oxidation of nitrite is accomplished with chromate and oxygen via (10).



which could be a way to stabilize nitrite melts.

Several of these specific chemical properties will be discussed later in connection with the experimental results, particularly as items which suggest future work.

The corrosion behavior of six iron alloys in Hitec was evaluated at the anticipated maximum use temperature in the solar central receiver of 823K. Since the chrome content of steels has been shown to have the most influence on oxidation-corrosion resistance<sup>20</sup> due to the formation of Cr<sub>2</sub>O<sub>3</sub>, the alloys were chosen so that the chrome content systematically ranged from 0 to 25 wt.% and included a C-steel and stainless steels. The chemical compositions of the six metals studied are listed in Table I. Of the alloys chosen, those with < 9% Cr are relatively inexpensive materials currently used in structural configurations for steam boilers. They may be equally appropriate for solar

---

\*Cr<sub>2</sub>O<sub>7</sub><sup>2-</sup>/CrO<sub>4</sub><sup>2-</sup> buffers for oxide have been added to such melts for other reasons as well<sup>19</sup>.

central receiver designs. The low C steel was used to determine the baseline for Cr influence.

### Experimental Technique

The immersion bath sketched in Figure 1 was built for testing the alloys in molten Hitec salt. Six coupons of each alloy were weighed and immersed in the molten salt. The samples had the approximate surface areas and dimensions listed in Table II, and all the samples were polished to 600 grit finish on one side. The Cr-2, Cr-5, and Cr9-1M samples were curved because they were cut from tubing. The Hitec mixture was prepared from reagent grade (> 98% pure)  $\text{NaNO}_2$ ,  $\text{NaNO}_3$  and  $\text{KNO}_3$ . The samples were kept in the bath at 523K (just above the melting point of the salt) for 5 days while the apparatus was being tested, and then the temperature was raised to the test temperature, 823K. The initial immersion at 523K for 5 days caused negligible oxidation. Samples of each alloy were withdrawn from the salt bath after 35, 108, and 190 days of exposure to molten Hitec at 823K and were not returned to the bath. The samples were weighed, inspected optically and with the scanning electron microscope for topographical features. Metallographic cross sections were made of each alloy before and after corrosion. In addition, electron microprobe studies and x-ray analyses were performed on selected samples.

The metal samples were placed on quartz racks (to electrically insulate one sample from another) in a pyrex container for the duration of the experiment. The quartz and pyrex were attacked during the experiment as expected from the strong basic character of the melt. The salt baths were kept in ambient air with a loosely fitting cover glass that was also etched during the experiment. The beaker was attacked mostly below the liquid level. The cover glass had a basic (high pH) deposit on its underside. No increase in the silica or boron content of the salt due to dissolution of the glass was observed.

### Results and Discussion

Table III and Figures 2-4 summarize the weight changes that occurred during the tests. All metals showed a weight gain due to oxide formation. The 1018 and stainless steel alloys gained weight continuously over the 190 day period. In contrast, the Cr-2, Cr-5, and Cr9-1M alloys gained weight initially but then did not gain more weight. Some of the scatter in data was caused by spalling of the oxide scale.

Regions of locally adherent and well bonded oxide were observed on every alloy. This is illustrated in the macro photo of Figure 5 and the metallographic cross-sections of Figure 6. Only the stainless coupons had oxide layers which were adherent throughout. In no case was intergranular corrosion or internal oxidation observed. X-ray diffraction of the scales of Cr-2, Cr-5, Cr-9 samples showed that both  $\text{Fe}_3\text{O}_4$  and  $\text{Fe}_3\text{O}_3$  were present. The oxides of the other coupons were too thin for x-ray analysis. These results are

consistent with previous studies. Passivation of iron in molten nitrate salts has been observed, and attributed to the formation of a mixed film that is primarily  $\text{Fe}_3\text{O}_4$ <sup>4,5,7</sup>. Continuous, adherent, blue-black films were found on iron in less than 100 minutes, when submerged in  $\text{NaNO}_3$ ,  $\text{NaNO}_2$ , and an equimolar mixture of  $\text{NaNO}_3$  or  $\text{KNO}_3$ <sup>5</sup>. Dissolution of iron has not been observed in mixed molten  $\text{NaNO}_3$ - $\text{KNO}_3$ <sup>4</sup>; however, dissolution was seen in another case of mixed nitrates<sup>13</sup>, and intergranular attack was observed with 330 stainless steel<sup>4</sup>. Mixed oxide scales are also found on Fe oxidized in air<sup>22,23</sup>.

The effect of chromium is illustrated in Figure 4 where the oxidation of each alloy is plotted versus the chrome content of the alloy as the chromium content varies from 0 to 25 weight percent. The beneficial effects of chromium on retarding corrosion in molten Hitec are clear. The variation in the amount of oxidation spans two orders of magnitude. In other oxidation experiments<sup>23B</sup> molybdenum enhanced oxidation resistance; thus, molybdenum may have contributed to the improved behavior of the Cr9-1M compared to the lower Cr alloys.

Visual inspection showed that the Cr-2 performed the poorest, as is apparent in the macrophotograph of the 190 day samples in Figure 5. Spalling and orange-colored blisters were present on all the Cr-2 samples. Some craters were also observed on the 1018, Cr-5, and Cr9-1M samples. The stainless steel samples did not spall or blister. All the metal coupons turned very dark grey in the salt.

Topographical scanning electron microscope (SEM) photographs of the oxide scales on the metal coupons revealed some interesting characteristics of the oxide scales (see Figure 7). The stainless steel coupons had small ( $< 5 \mu\text{m}$ ), equiaxed, dense crystals on the surface. The lower chrome alloys had slightly larger grains, and many of the grains were split into laminar plates. Cracks between the laminar plates could have been paths for diffusion of Fe or oxygen, and could have caused the low chromium alloys to corrode faster than the stainless steel.

An automated electron microprobe X-ray analyzer<sup>24,26</sup> was used to determine the chemical composition of the corrosion layers of a 5% Cr sample and a 316 sample. The microprobe was programmed to collect elemental X-rays from 1600 points in an  $80 \mu\text{m} \times 80 \mu\text{m}$  square matrix centered on the metal-oxide interface of a polished metallographic cross-section. Using a computer program called QEMCA<sup>25</sup> the X-ray intensities of each point in the matrix were corrected for X-ray absorption, fluorescence, and atomic number. The corrected X-ray intensities were used to produce a computer-generated map of each element of interest. Figure 8 is a series of computer images from the Cr-5 alloy that displays the relative elemental distribution of the Fe, Cr, and oxygen. Figure 9 is a typical quantitative profile of Fe, Cr, and oxygen showing the variation of the Cr and Fe in the oxide layer adjacent to the metal-oxide interface. The outermost half ( $\sim 20 \mu\text{m}$ ) of the oxide layer is entirely Fe-oxide. Due to lack of an adequate Fe/Cr-oxide standard, the weight percents in the profiles of Figure 9 do not conform to the standard Fe/O ratios of  $\text{Fe}_3\text{O}_4$ , FeO, or  $\text{Fe}_2\text{O}_3$ . The weight percentages decrease at the samples outer edge due to imperfections in the mounting.

The microprobe was also used to study a 316 stainless steel metal-oxide interface. There were problems in locating the oxide metal interface because

the oxide was very thin; however, there was evidence that the outermost oxide was entirely Fe-oxide and the inner layer enriched with Cr, Ni, and perhaps Mo. A chromium-rich inner layer has also been observed in the oxidation of Fe alloys<sup>2,27</sup>. Oxidation protection is initially by Cr<sub>2</sub>O<sub>3</sub> or an Fe-Cr-O spinel formation which subsequently breaks down and an Fe-rich oxide outer layer forms<sup>27</sup>.

The oxidation of metals has been extensively studied, and the reader is referred to References 22 and 23 for more complete discussion. Metals may oxidize by several mechanisms; however, parabolic oxidation has been observed for Fe and Fe alloys in air and oxygen<sup>22</sup>, and in short-term test with molten nitrates<sup>4,6</sup>. Parabolic behavior conforms to Equation (11) below where t is time. K<sub>p</sub> and b are constants.

$$(\Delta \text{weight})^2 = K_p t + b \quad (11)$$

The results were not sufficiently precise to be modeled quantitatively, but some qualitative features will be discussed. Assuming parabolic behavior for the 1018 steel and the two stainless alloys, values of K<sub>p</sub> and b were calculated for each. K<sub>p</sub> ranged from 0.001 to 0.09 mg<sup>2</sup>/cm<sup>4</sup>/day. The rate constant, K<sub>p</sub> decreased with increasing chromium content. Parabolic oxidation rate constants from the literature are listed with those from this study in Table IV. The rate constants derived from the shorter term experiments in the literature are higher than those based on the present work. The parabolas shown in Figure 2 for the 1018, 316, and 310 alloys were very flat. It is hypothesized that a very rapid oxidation process took place early in the experiment and cannot be described with this limited data; the rapid process was followed by a slower oxidation process. Consistent with this speculation is the fact that Baraka<sup>5</sup> observed two parabolic oxidation mechanisms within 10 hours at 723K with a KNO<sub>3</sub>-NaNO<sub>3</sub> eutectic.

The salt composition changed over the six months of the experiments (see Table V). The amount of nitrite (NO<sub>2</sub>) decreased significantly. A carbonate analysis of the last salt sample showed that the Hitec was reacting with the CO<sub>2</sub> of the atmosphere to form Na<sub>2</sub>CO<sub>3</sub> and K<sub>2</sub>CO<sub>3</sub>. Also, the etching of the glass equipment that occurred reflected the strong base nature of the melt. The changes in composition may not have altered the corrosion process significantly since NaNO<sub>2</sub> behaved similarly to NaNO<sub>3</sub> in other corrosion tests with iron<sup>5</sup>. The Na/K ratio was reasonably constant throughout the experiment, eliminating any effect due to preferential mass transport of Na or K out of the bath, e.g., by vaporization or NaOH(g) formation. The concentration of other metals did not change during the experiment. The presence of oxygen, water, acids or bases in molten nitrate melts have been shown to have minimal effect on the corrosion behavior of iron<sup>3,4</sup>.

Since it has been seen that alloys corrode by an oxidation process when immersed in nitrate salts, it is of interest to compare the effects of air (where more data are available) and nitrates. Figure 10 shows the results of some long-term (42 day) oxidation experiments at 900K in air<sup>23B</sup> along with the results of the present experiment (35-day exposure at 823K). The results in Hitec are of the same order of magnitude as the oxidation experiments

performed in air. However, given that the air experiments were carried out at higher temperatures and for longer times, it is reasonable to conclude that the oxidation of metals in Hitec is slightly more rapid than in air. This is supported by Notoya's results<sup>3</sup> and is consistent with the hypothesis that oxidation mechanisms are similar in any oxidant but the rates are media dependent<sup>27</sup>.

All of the alloys tested showed reasonable resistance to the molten salt. From chemical corrosion considerations only, the stainless alloys are good candidates for the highest temperatures of a solar central receiver, i.e., in the receiver. The Cr-2 alloy is not an acceptable choice for use with molten Hitec at 823K due to its oxidation, spalling and blistering. The 1018, Cr-5 and Cr9-1M are candidate materials that are worthwhile investigating for lower temperature applications, especially where cost is a critical consideration (as in large storage tanks).

This was the first of a series of experiments that address chemical corrosion in molten nitrate salts for solar central receiver applications. Current experiments are underway to test the same alloys immersed in Hitec at 773 and 723K. In addition, these alloys are being tested in (54 wt.%  $\text{KNO}_3$ -46 wt.%  $\text{NaNO}_3$ ) another heat transfer salt candidate in the same temperature regime.

### Conclusions

The six iron alloys tested in molten Hitec at 823K formed oxide layers within one month. The amount of oxidation spanned two orders of magnitude and was strongly dependent on Cr content. The C-steel and 316 and 310 stainless steels conformed to parabolic oxidation kinetics with rate constants equal to 0.09, 0.0028, and 0.0011  $\text{mg}^2/\text{cm}^4/\text{sec}$ , respectively. Electron microprobe studies showed Fe and Cr gradients in the oxide of a 5% Cr alloy, with an outermost Fe-rich oxide. The behavior of the low Cr alloys was similar to oxidation in air.

This screening experiment indicated that commercial Fe alloys are suitable for use in solar central receiver designs using Hitec salt at temperatures up to 823K. Stainless steels are particularly resistant to corrosion at 823K.

# MOLTEN SALT BATH

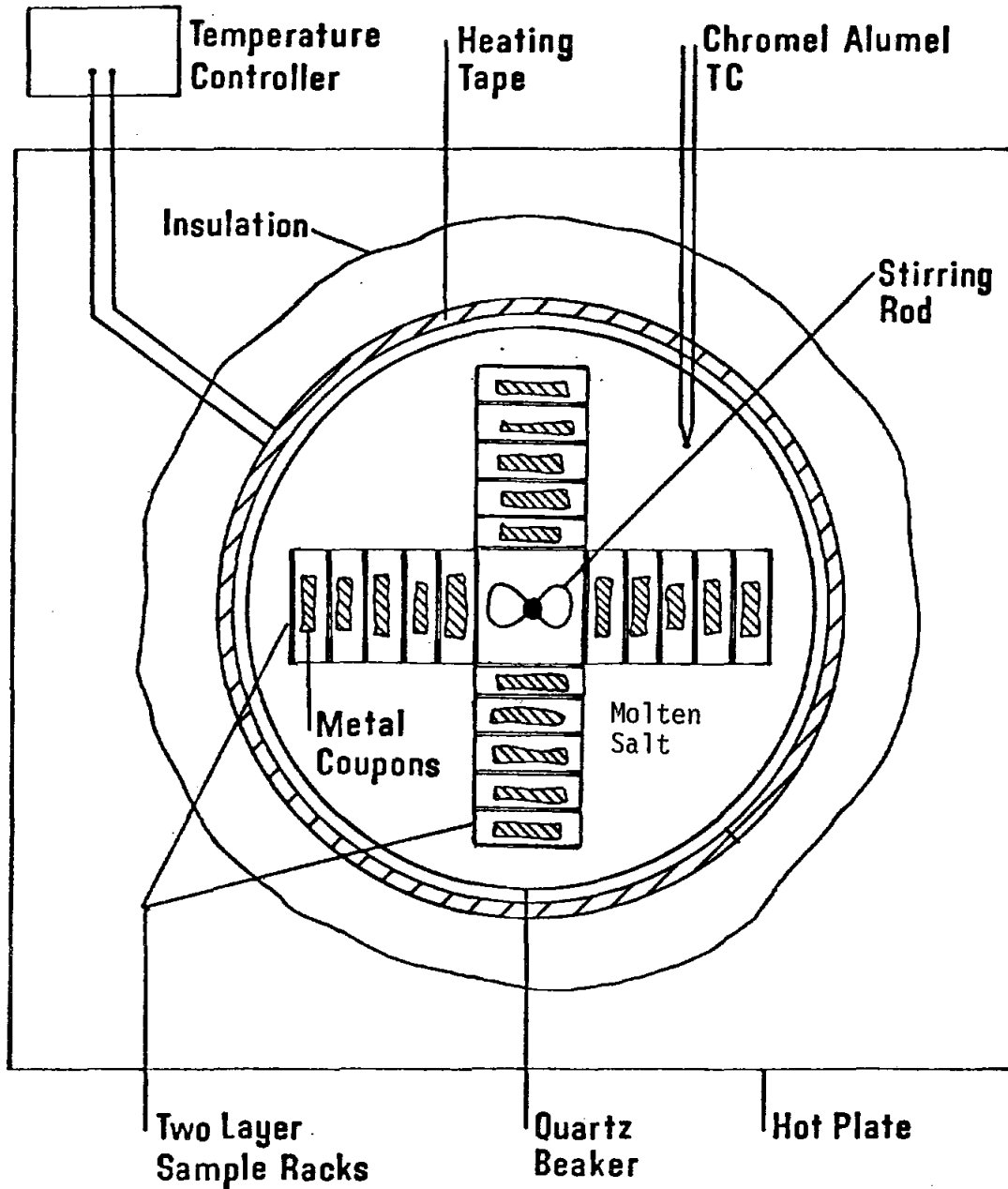


Figure 1. A schematic of the submersion bath used for corrosion screening in molten salt. (Viewed from the top)

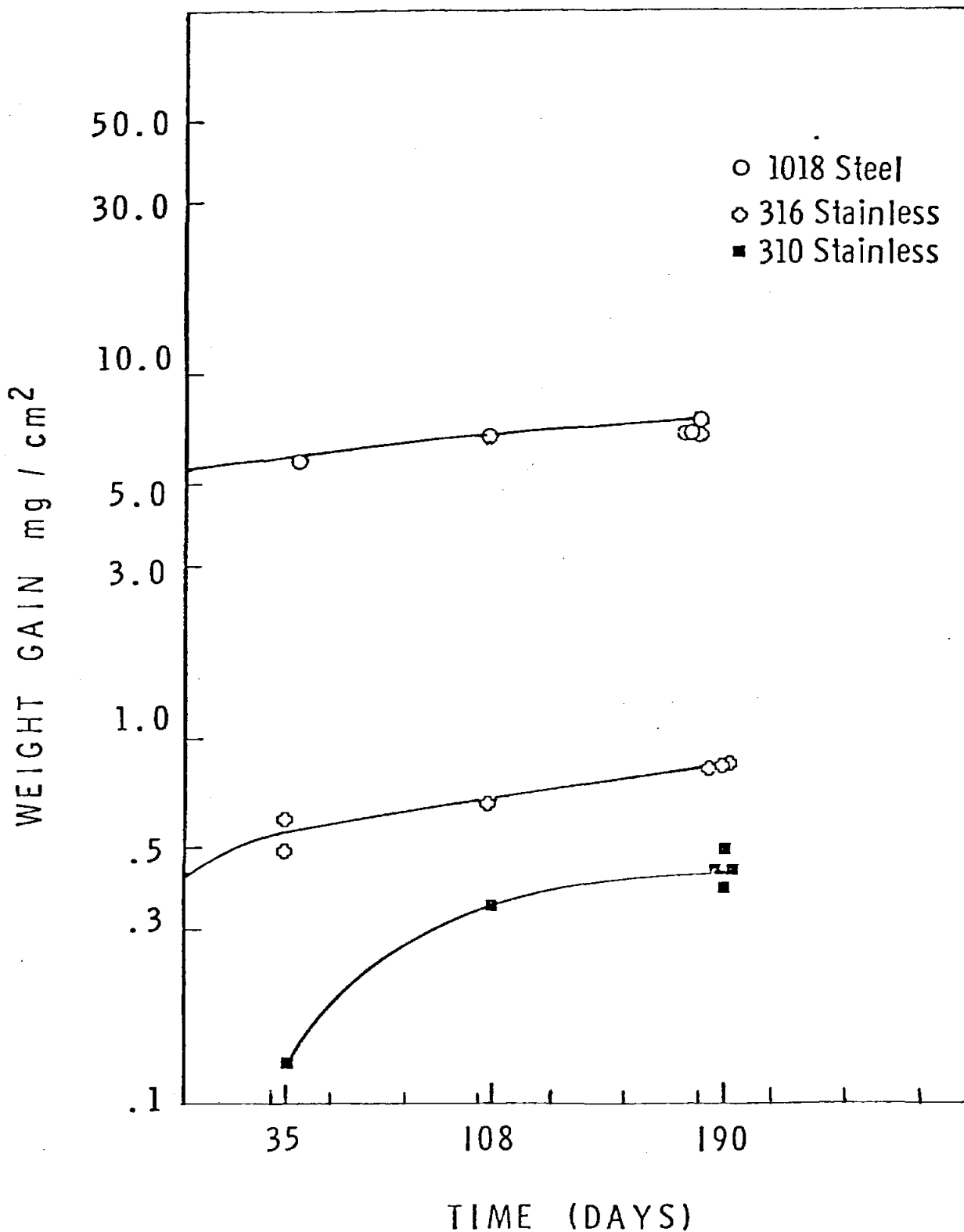


Figure 2. The total weight gains for 1018 steel and two stainless steels are plotted versus time. The data points were fitted to parabolic curves which are shown in the figure. Each data point represents one metal coupon.

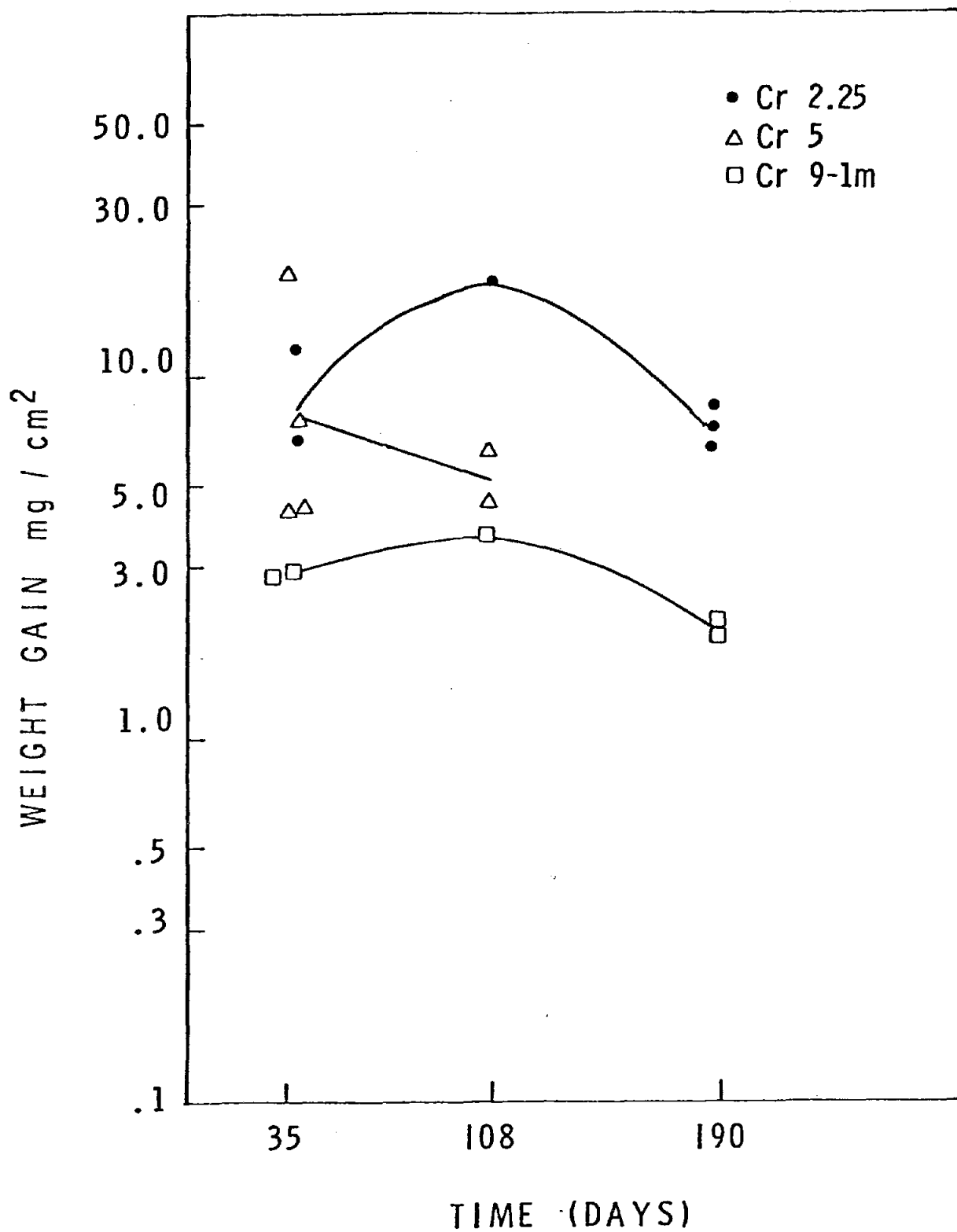


Figure 3. Total oxidation for 3 low-Cr Fe alloys is plotted here with respect to time. The scatter in the data is due to spalling and errors in the estimated surface area. Each data point represents 1 coupon.

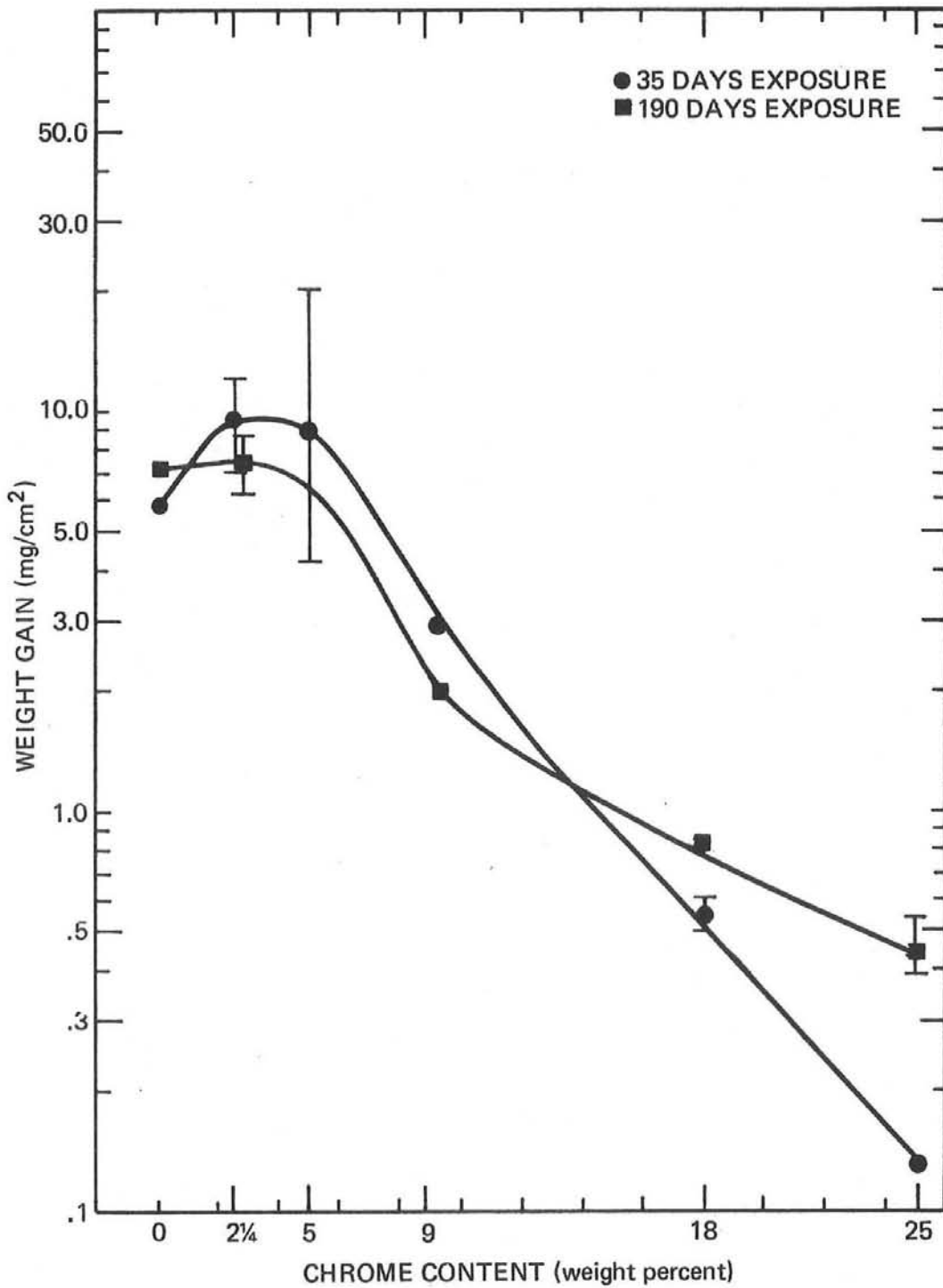


Figure 4. The Oxidation of Fe alloys is plotted versus chromium content in this figure. Spalling of oxide may have contributed to spurious results in the low Cr alloys where the apparent oxidation is less after 190 days than after 35 days. Chromium content has a larger effect initially than after longer times.

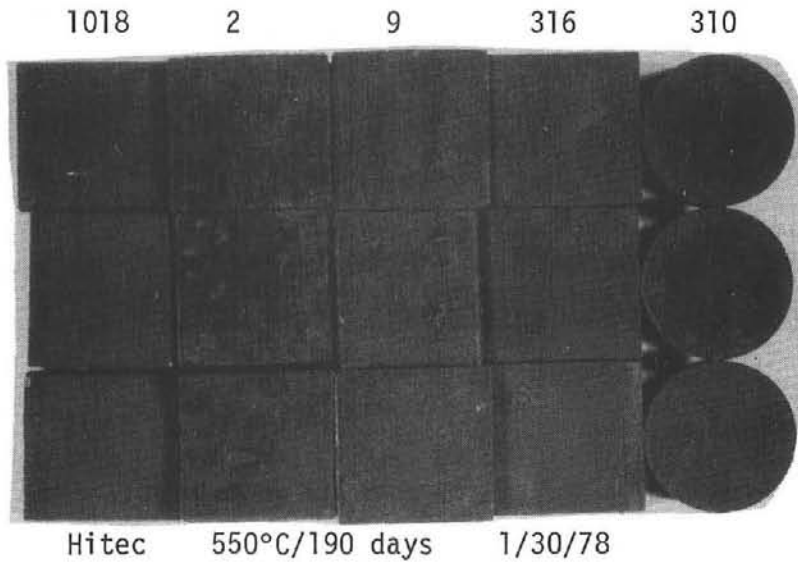


Figure 5. Macro photo of metal coupons that had been immersed in molten Hitec salt at 823K for 190 days. The coupons are (from L to R in columns) 1018 steel, Cr-2, Cr9-1M, 316 stainless and 310 stainless.

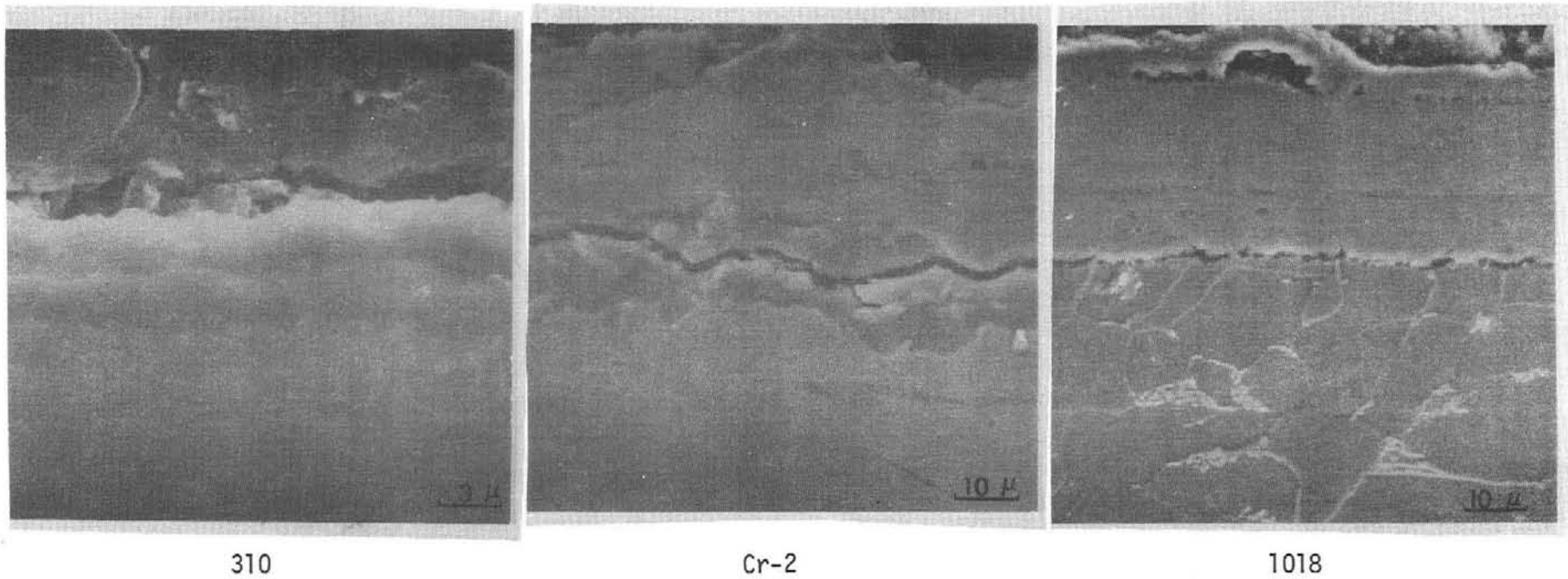
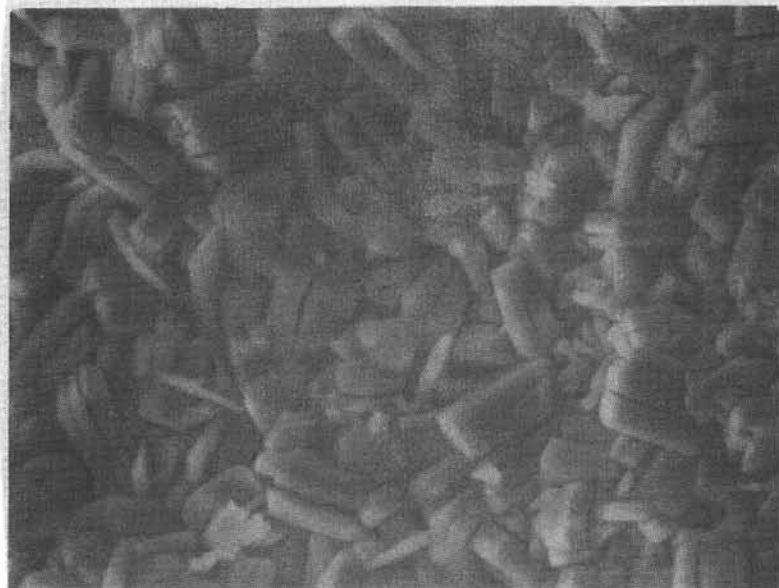


Figure 6. Crosssectional photo of selected corrosion coupons. From the right they are 1) 1018 steel, 2) Cr-2, and 3) 310 stainless. The base metal is at the bottom and the oxide is above. No intergranular corrosion or internal oxides were observed.



10  $\mu\text{m}$

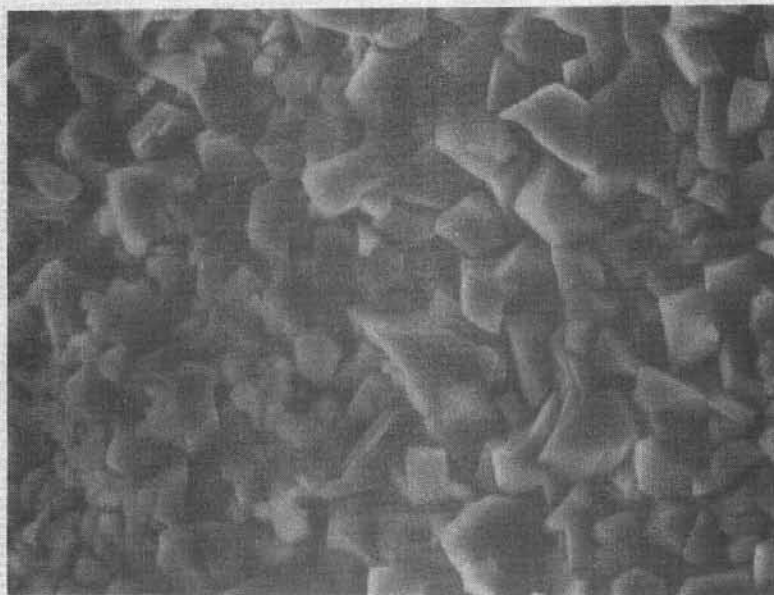


Figure 7. Topographical photos of Cr9-1M (top) and 310 stainless (bottom) after oxidation in Hitec salt at 823K for 190 days. The Cr9-1M scale shows much cracking in the oxide film that enhances oxidation.

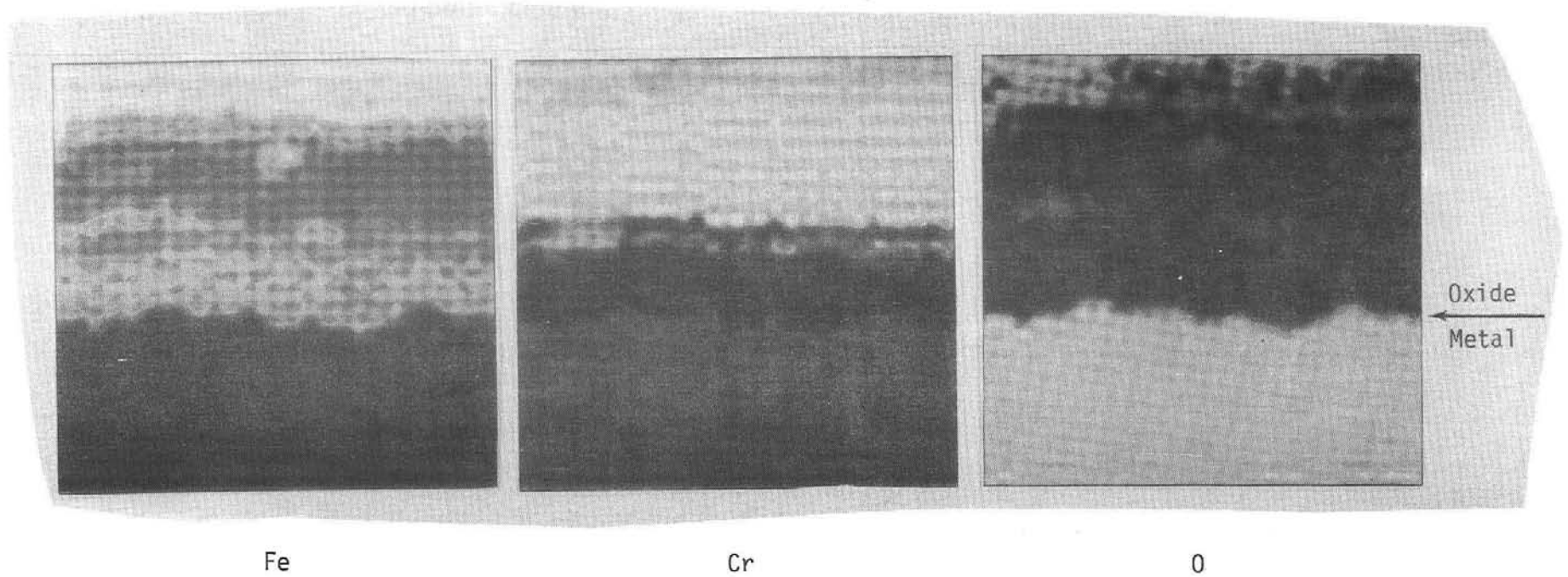


Figure 8. Computer generated images map the intensity of 3 elements, Fe, Cr, and oxygen over the same area of oxide-metal interface. Darker color indicates greater concentration.

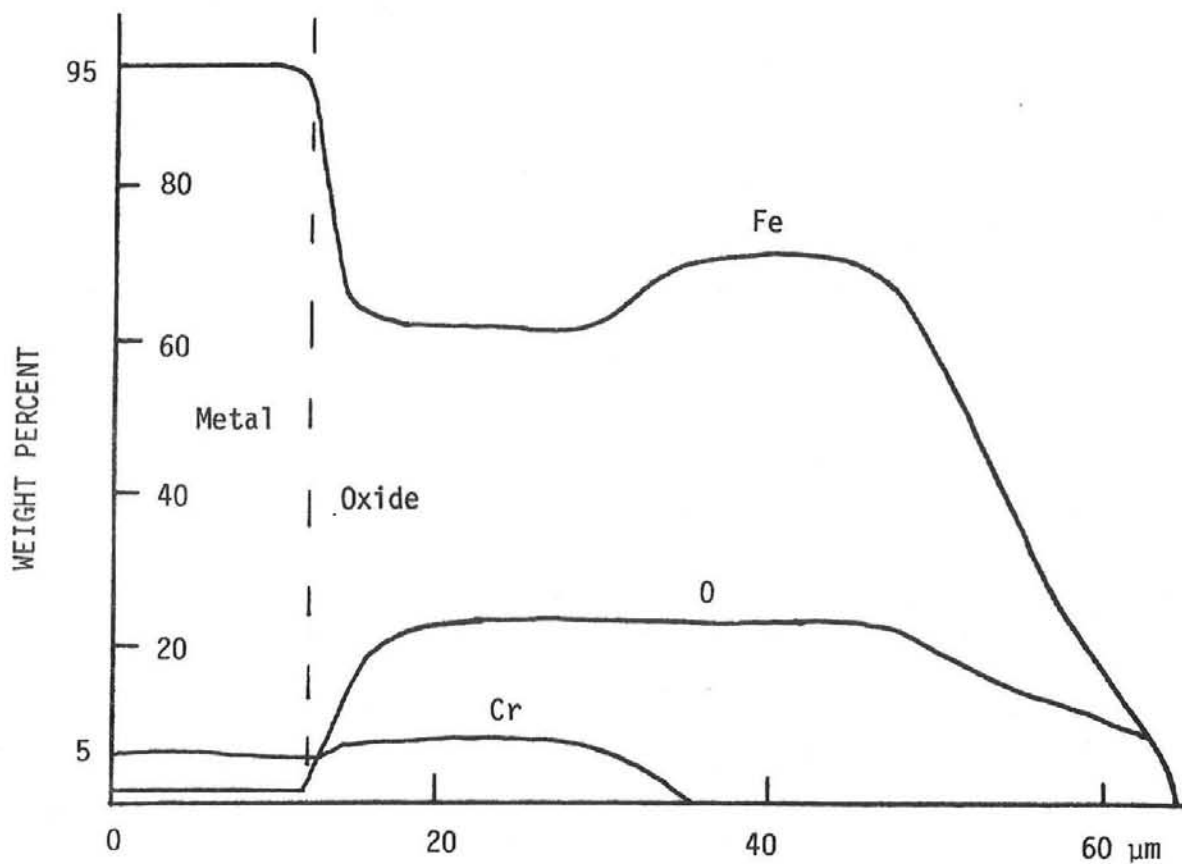
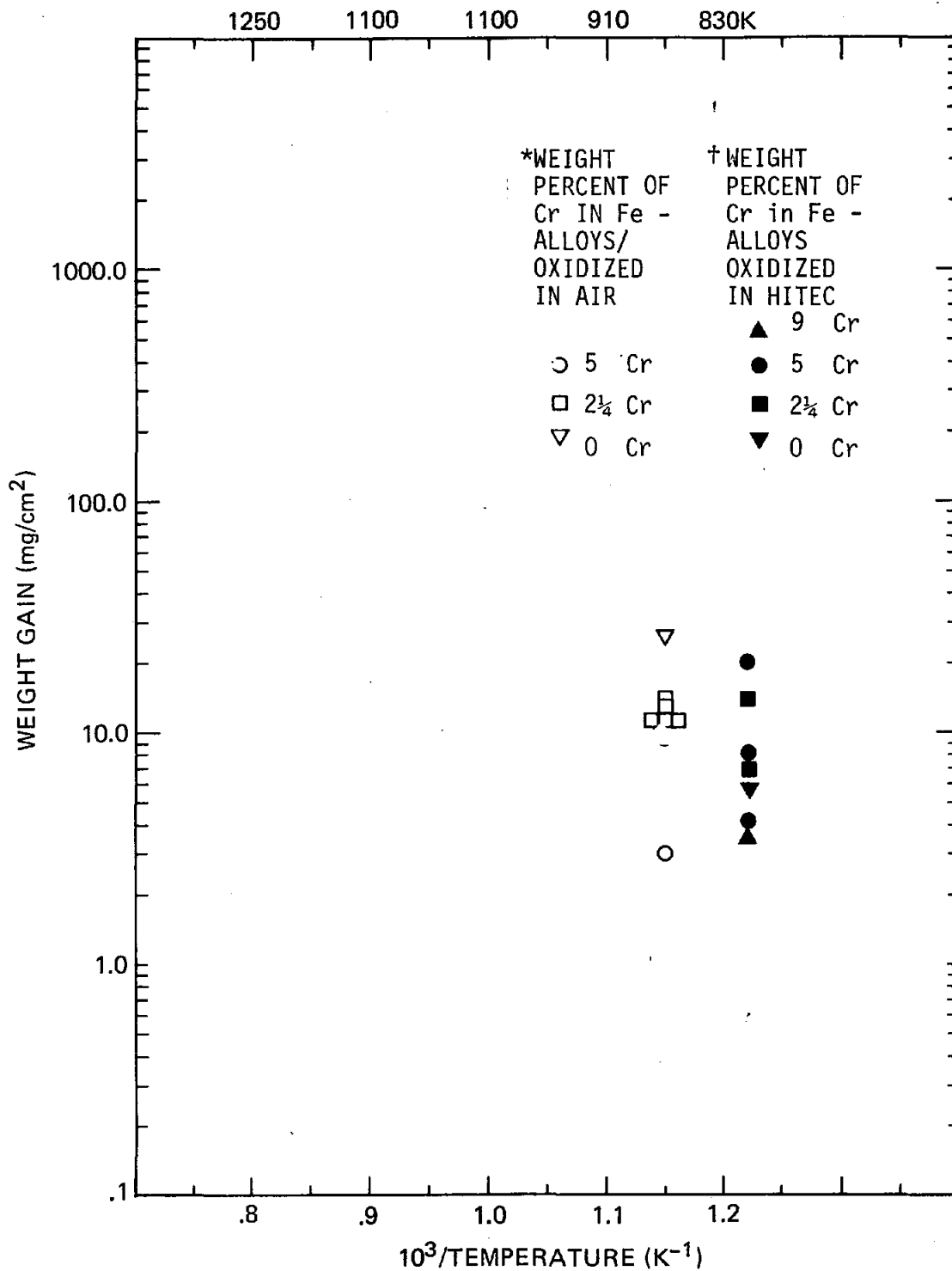


Figure 9. Electron probe concentration profiles of Cr-5 oxide/metal interface (after oxidation in Hitec salt at 823K for 190 days) above illustrate the Cr-rich layer adjacent to the metal. Pure Fe oxide is present at the outer edge.

Figure 10. Oxidation of Fe-Cr alloys in air and Hitec.



\*Oxidized in Air for 1000 hrs  
(Reference 10b)

†Oxidized in Hitec for 850 hrs  
(This Study)

TABLE I  
 CHEMICAL COMPOSITION OF ALLOYS CHOSEN FOR  
 IMMERSION TESTING IN MOLTEN HITEC (WT%)

<u>Alloy</u>	<u>Cr</u>	<u>C</u>	<u>Ni</u>	<u>Mn</u>	<u>Mo</u>	<u>Si</u>	<u>Fe</u>
1018 Steel	0.	0.15-0.2	-	0.6-0.9	-	<0.5	balance
Cr-2	1.9-2.6	<0.15	-	0.3-0.6	0.5	<0.5	balance
Cr-5	5.13	<0.12	-	0.44	0.5	0.37	balance
Cr 9-1M	8.-10.	<0.15	-	0.3-0.6	0.9-1.1	<1.0	balance
316 Stainless	16.-18.	<0.08	10.-14.	<2.0	2.-3.	<1.0	balance
310 Stainless	24.-26.	<0.25	19.-22.	<2.0	-	<1.5	balance

TABLE II  
 SAMPLE DIMENSIONS FOR HITEC CORROSION TESTING

<u>Alloy</u>	<u>Dimensions (mm)</u>	<u>Surface Area (cm<sup>2</sup>)</u>
1018 Steel	25 x 25 x 7	19.4
Cr-2*	25 x 25 x 8	20.6
Cr-5*	25 x 25 x 7	19.4
Cr9-1M*	25 x 25 x 7.5	20.0
316 Stainless	25 x 25 x 7	19.4
310 Stainless	25 diam. x 7	15.2

\*Dimensions are approximate since samples were curved pieces cut from 15 cm diameter tubing.

TABLE III

TOTAL OXIDATION (WEIGHT GAINS) OF Fe  
ALLOYS AFTER IMMERSION IN HITEC SALT AT 820K

<u>Alloys</u>	<u>After 35 Days</u>	<u>After 108 Days</u>	<u>After 190 Days</u>
1018	5.7 mg/cm <sup>2</sup>	6.8 mg/cm <sup>2</sup>	6.8 mg/cm <sup>2</sup> 6.9 6.9 7.4
Cr-2	6.8 11.9	17.8	6.2 7.2 8.7
Cr-5	4.2 4.3 8.0 20.	4.7 5.6	*
Cr 9-1M	2.8 2.9	3.6	1.8 2.1
316 Stainless	0.49 0.59	0.66	0.84 0.85 0.87
310 Stainless	0.13	0.35	0.37 0.42 0.42 0.53

\*No sample available

TABLE IV  
RATE CONSTANTS FOR OXIDATION OF IRON ALLOYS

<u>Reference</u>	<u>Temperature (K)</u>	<u>Duration of Experiment (hrs)</u>	<u>Media</u>	<u>Material</u>	$K_p \left( \frac{\text{mg}^2}{\text{cm}^4 \text{ sec}} \right)$	$b \text{ (mg}^2/\text{cm}^4)$
This Study	823	4506	Hitec	1018 Steel	0 .09	5.6
This Study	823	4506	Hitec	316 Stainless	0 .0028	0.43
This Study	823	4506	Hitec	310 Stainless	0 .0011	-0.11
3	823	8	KNO <sub>3</sub>	Fe	2.1	†
3*	823	8	NaNO <sub>3</sub>	Fe	8.6	†
3*	823	8	(Na/K)NO <sub>3</sub>	Mild Steel	150.	†
11A	773	100	O <sub>2</sub>	Fe-0.1C	0.48	†

\*Extrapolated from lower temperatures

†Not reported

TABLE V  
 CHEMICAL COMPOSITION OF MOLTEN SALT BATH  
 USED FOR CORROSION TESTING AT 820K

	<u>Na/K</u> <sup>†</sup>	<u>NO<sub>2</sub>/NO<sub>3</sub></u> <sup>†</sup>	<u>CO<sub>2</sub></u> <sup>*</sup>
Starting Salt	0.72 ± 0.05	0.49 ± 0.05	nm
After 35 days at 820K	0.83	0.18	nm
After 108 days at 820K	0.78	0.074 ± .01	nm
After 190 days at 820K	0.78	0.040	0.17

\*Weight percent, representing reaction with water, carbon dioxide and decomposition to the oxide.

†Based on weight ratios.

## ACKNOWLEDGMENTS

The authors are very appreciative of the work many people have contributed to this project. Larry Stephensen set up and operated the salt baths. Tommie Bryant and Dave Geene did the metallographic work. Clarence Karfs did the SEM work. Cal Feemster and Suzanne Deutscher facilitated the chemistry analysis. Thanks also to Chris Wilson, Pete Dean and Bob Bradshaw.

## REFERENCES

1. A) T. D. Brumleve, High-Temperature Solar Energy System, SAND74-8008.  
B) A. C. Skinrod, T. D. Brumleve, C. T. Schafer, C. T. Yokomizo, C. M. Leonard, Status Report on a High Temperature Solar Energy System, SAND74-8017.  
C) T. D. Brumleve, Status Report on the Direct Absorption Receiver, SAND78-8702.
2. Hitec Heat Transfer Salt, DuPont Bulletin.  
W. E. Kirst, W. M. Nagle, J. B. Castnen, AIChE Trans, 36, 371, 1941.
3. T. Notoya, R. Midorikawa, Denki Kagaku, 39, (12), 930, 1971.
4. A. J. Arvia, J. J. Podesta, R. C. V. Piatti, Electrochem Acta, 17, 33, 1972.
5. A. Baraka, A. I. Abdel Rohman, A. A. El Hosary, Brit. Corros. J., 11, (1), 44, 1976.
6. E. I. Gurovich, Zh Prikl. Khim., 29, 1358, 1956.
7. I. D. Dirmeik, Corrosion NACE, 25, (4) 180, 1969.
8. S. L. Marchiano, A. J. Arvia, Electrochem. Acta, 17, 861, 1972.
9. A. J. Arvia, J. J. Podesta, and R. C. V. Piatti, Electrochem. Acta 16, 1797 (1971).
10. H. E. Bartlett and K. E. Johnson, Corrosion Science 6, 87 (1966).
11. J. A. Plambeck, J. Chem. Engr. Data 12, 77 (1967).
12. L. G. Boxall and K. E. Johnson, J. Electroanal. Chem. 30, 25 (1971).
13. A. Plambeck in Encyclopedia of Electrochemistry of the Elements, Volume X, Fused Salt Systems, Allen J. Bard, Editor, Marcel Dekker, New York, N.Y., 1976.
14. S. L. Marchiano and A. J. Arvia, J. Appl. Electrochem. 4, 191 (1974).
15. E. S. Freeman, J. Am. Chem. Soc. 79, 839 (1957).
16. R. F. Bartholomew, J. Phys. Chem. 70, 3442 (1966).

17. P. G. Zambonin, Anal. Chem. 44, 763 (1972).
18. J. Alexander, Jr. and S. G. Hindin, Ind. Engr. Chem. 39, 1044 (1947).
19. D. A. Nissen, Sandia Laboratories, Private Communication.
20. Corrosion Resistance of the Austenitic Cr-Ni Stainless Steels in High Temperature Environments, INCO Publication A-320 5M 3-76, One New York Plaza, NY, NY 10004.
21. Encyclopedia of Electrochemistry of the Elements, 10, J. A. Plambeck, ed. A. J. Bard, Marcel Dekker Inc., NY, 1976.
22. A) D. Caplan, et al., Oxidation of Metals, 12 (1) 67, 1978.  
B) L. B. Pfeil, J. Iron & Steel Inst., 123, 237, 1931.  
C) Corrosion and Oxidation of Metals, U. R. Evans, Edward Arnold, London, 1960.  
D) O. Kubaschewski, B. E. Hopkins, Oxidation of Metals and Alloys, 2nd ed., Butterworth & Co., London, 1962.
23. A) D. Inman, N. S. Wrench, Brit. Corros. J., 1, 246, 1966.  
B) Corrosion, V.1., ed. L. L. Shreir, Newnes-Butterworths, London, 1976.  
C) Corrosion Resistance of Metals and Alloys, 2nd ed., ed. F. L. Laque, Reinhold Pub. Co., NY, 1963.
24. W. B. Estill and D. E. Benthussen, "Practical Aspects of Microprobe Automation," Proc. 8th Electron Probe Analysis Society (1973).
25. D. E. Benthussen, W. B. Estill, Application Software for Electron Microprobe Analysis and Data Reduction, SLL-74-0005 (1974).
26. W. B. Estill, H. Jones, and G. Miller, (to be published).
27. L. A. Morris, Met. Eng. Qtrly, 30, May 1968.

UNLIMITED RELEASE

INITIAL DISTRIBUTION:

Bob Lessley  
Bechtel National, Inc.  
P. O. Box 3965  
San Francisco, CA 94119

Larry Manuel  
5246 Desmond St.  
Oakland, CA 94618

Z. A. Munir  
UC Davis  
Davis, CA 94616

O. Scott  
Denver Division  
Martin Marietta Aerospace  
P. O. Box 179  
Denver, CO 80101

A. J. Slemmons  
SRI  
333 Ravenswood Ave.  
Menlo Park, CA 94025

Tom Tracy  
Denver Division  
Martin Marietta Aerospace  
P. O. Box 179  
Denver, CO 80101

D. Douglass, 5831  
N. Magnani, 5831  
W. H. Smyrl, 5831 (5)  
E. Beauchamp, 5846  
T. B. Cook, Jr., 8000; Attn: A. N. Blackwell, 8200  
M. Brown, 8162  
B. F. Murphey, 8300  
D. M. Schuster, 8310  
D. R. Adolphson, 8312  
R. W. Bradshaw, 8312  
C. M. Kramer, 8313 (15)  
R. W. Mar, 8313  
W. R. Hoover, 8314  
S. L. Robinson, 8314  
L. A. West, 8315  
J. Swearingen, 8316  
W. B. Estill, 8316 (5)  
L. Gutierrez, 8400  
S. L. Roche, 8342  
T. D. Brumleve, 8451

W. Wilson, 8451  
J. J. Bartel, 8452  
L. Radosevich, 8452  
A. C. Skinrod, 8452  
L. N. Tallerico, 8452  
J. Gilson, 8453  
F. J. Cupps, 8265/Technical Library Processes Division, 3141  
Technical Library Processes Division, 3141 (2)  
Library and Security Classification Division, 8266-2 (3)  
Technical Publications and Art Division, 8265, for TIC (27)